11TH INTERNATIONAL SCIENTIFIC CONFERENCE
ON DEFENSIVE TECHNOLOGIES
OTEH 2024
Serbia, Tara, 9-11 October 2024

CATALYTIC PROPERTIES OF PAPER-IMMOBILIZED HORSE SERUM BUTYRYLCHOLINESTERASE

SONJA BAUK
Military Technical Institute, Belgrade, bauk.sonja@gmail.com

NATAŠA PAJIĆ
Military Technical Institute, Belgrade, natasa.pajic969@gmail.com

Abstract: *Fast and reliable detection of toxic organophosphates (OPs) is an important safety issue due to their widespread application, extreme toxicity and potential use as chemical warfare agents. Recently, paper has attracted considerable attention as inexpensive, biodegradable, biocompatible and hydrophilic material, which is owing to its unique features very suitable matrix for fabrication of fast-responding and low-cost analytical tools in health and environmental applications. Bioactive paper sensors with immobilized enzymes that enable colorimetric readout are used for naked-eye detection and able to operate without sophisticated equipment. Cholinesterases (ChEs) are enzymes susceptible to inhibition by OPs with high sensitivity and this property enabled the invention of simple detectors and disposable analytical devices for OPs assay. This work reports simple and cost-effective immobilization of commercial horse serum butyrylcholinesterase (BChE) on paper-based matrix and describes the catalytic properties of the immobilized enzyme relevant from some practical aspects related to storage and operating conditions.*

Keywords: *butyrylcholinesterase, organophosphates, immobilization, cellulose, detection.*

1. INTRODUCTION

The immobilization of enzymes from the cholinesterase (ChE) family is the most important step in the design and fabrication of various bioanalytical tools that are widely used in many areas, including life science research, drug discovery, clinical diagnostics, environmental monitoring, food safety control, forensics and military defense [1]. Their function is based on enzyme inhibition, since their output signals, according to a measurable property, correspond to the activity of the immobilized enzyme, which decreases after exposure to the target analyte.

The application of immobilized ChEs in such a large number of different fields is due to the wide variety of species exerting the anti-ChE effect. ChE inhibitors, as target analytes of ChE-based analytical tools, comprise a diverse group of compounds such as glycoalkaloids, aflatoxins, anatoxins, organophosphate and carbamate pesticides, nerve agents, anti-Alzheimer drugs, heavy metals and several others [2]. Among others, one of the main and most widespread applications of immobilized ChEs is aimed at the determination of toxic organophosphates (OPs). Although these compounds are very harmful for wildlife and human health and the most toxic of them belong to the group of chemical warfare agents (CWAs), they are still intensively used for agricultural, industrial, household and medical purposes. The health risks and threats to life associated with their use trigger the need for reliable, fast and inexpensive analytical systems that can enable the early detection of this type of environmental contaminants [3].

So far, a large number of different biosensing platforms have been proposed for a range of ChE inhibitors, as this topic has been the subject of many research and development activities over several decades. In addition to electrochemical, photoelectrochemical, optical and piezoelectric biosensors with signal acquisition that mainly relies on instruments, considerable efforts in this field are directed towards inventing simple detectors and disposable analytical devices, which are particularly suitable for military, environmental and agricultural purposes [4][5]. They are often designed in the form of various tubes, dipsticks and strips and able to operate without any instrumental device, since their work relies on the colorimetric readout method. This method provides a visual color change as an analytical signal that is observable by the naked eye or can be evaluated using smartphones and available applications and software to convert captured images into corresponding data [6][7].

Regardless of whether it is a very simple device or a more complex one, the selection and effectiveness of the enzyme immobilization method are crucial for its performances and determine its storage and operating conditions. Over the past decades, various techniques have been applied for immobilization of ChEs from different sources on supports made of different materials, but there is no immobilization strategy without certain limitations and drawbacks [8]. Some of the most common disadvantages are related to process reproducibility, enzyme stability, desorption or leakage, loss of enzyme activity and product cost-effectiveness, but there are also many other issues whose resolution would contribute to certain improvements in this field. Enzyme

Corresponding author: S.Bauk;
E-mail: bauk.sonja@gmail.com
DOI: 10.5937/OTEH24097B

immobilization techniques can generally be divided into covalent and physical methods, according to the molecular forces between the enzyme and the support matrix, but combination of different techniques can often be found in the literature. Physical methods include adsorption and entrapment. They are simple, cost-effective and widely used due to the least effect on enzyme activity, which is the result of weak interaction with the carrier and the absence of chemical bonds.

The selection of a suitable immobilization technique in the fabrication of ChE-based analytical device depends on many different factors, taking into account its intended mode of operation, as well as the characteristics of the materials to be used for enzyme attachment. Considering the irreversible nature of ChEs inhibition by OPs and aforementioned trends towards simple testing devices, paper substrates have emerged as an attractive alternative to more sophisticated analytical platforms for this type of application. Paper is the most abundant and inexpensive cellulosic product that has recently attracted considerable attention as a matrix for fabrication of low-cost analytical tools. The immobilization of ChEs on paper surface led to the invention of various fast-responding tools for rapid screening and early diagnosis in health and environmental applications [9][10]. Paper-based biosensors provide rapid detection of OPs with minimal equipment requirements and with advantages of cost effectiveness, simple fabrication, disposability and stability.

Recently, we studied the application of a simple and cost-effective method for the immobilization of horse serum butyrylcholinesterase (BChE) on Whatman filter paper. In this work, two immobilizates obtained by the same technique were additionally examined, in order to gain a better insight into their properties relevant to some aspects related to their practical application.

2. MATHERIAL AND METHODS

2.1. Material

Lyophilized horse plasma butyrylcholinesterase (BChE, with the activity of ≥ 10 U/mg protein according to manufacturer's declaration), bovine serum albumin (BSA) and gelatin from porcine skin (high gel strength) were purchased from Sigma-Aldrich, as well as butyrylthiocholine iodide (BSChI, ≥ 99.0 %) and 5,5'-dithiobis (2-nitrobenzoic acid) (DTNB, ≥ 98 %). All other reagents were of analytical grade.

Filter paper Whatman No. 1 manufactured as circular disks with a diameter of 15 mm (paper circles) was used as a support matrix for enzyme immobilization.

Two different solutions containing BChE (~10 U/mL) and BSA (1 %) or gelatin (0.5 %) in phosphate buffer (PB, 50 mM, pH 7.4) were used to obtain two types of immobilizates (paper circles with immobilized enzyme), designated as ImA and ImG, respectively. The immobilization procedure consisted of applying the prepared enzyme solutions in aliquots of 20 μL to the surfaces of the paper circles, which after drying at laboratory temperature (25 ºC) were stored in closed glass vessels and kept in the refrigerator until use.

2.2. Activity assay

The BChE activity measurements were performed essentially according to the method of Ellman [11][11], using BSChI (2 mM) as the substrate and DTNB (0.32 mM) as the indicator (Ellman's reagent). Free enzyme (20 μL) was added to a cuvette containing PB (2.64 mL) preincubated at 25 ºC, followed by addition of DTNB (0.24 mL) and substrate (100 μL). The formation of the yellow anion obtained from the reaction between Ellman's reagent and the thiocholine generated by enzymatic hydrolysis of the substrate was monitored by measuring the linear increase in absorbance at 412 nm. The measurement of the immobilized enzyme activity was carried out as described above, except that one paper circle with immobilized BChE was taken instead of free enzyme and placed in a dry cuvette before all others reagents. All results were obtained by measurements performed in triplicate and measured values are presented as mean ± SD. One unit of enzymatic activity was defined as the amount of enzyme that catalyzes the hydrolysis of 1 μmol of butyrylthiocholine per minute.

2.3. Temperature effects on activity and stability

Bioactive papers with immobilized BChE were exposed to a temperature of 55 ºC for 2 hours in two different conditions: a) in an oven, where each sample was placed in a dry closed vessel, and b) in a water bath, where each sample was immersed in PB (2.64 mL) in a sealed cuvette. After the heat treatment, the samples were left at room temperature to cool slowly for the next 2 hours before each was transferred to a clean cuvette for the residual activity measurement by the standard assay method. The activity of PB remaining in the thermostated cuvette after sample removal was also determined, as well as the total activity in the cuvette containing the immersed sample in PB. The percentage of the residual activity was calculated considering the initial activity of the tested immobilizate before heat treatment as 100%.

2.4. The visual response's dependency on substrate concentration

The immobilized BChE activity was visualized with five test solutions (S1 – S5) containing DTNB (4 mM) and BSChI at concentrations of 1.5 mM (S1), 3 mM (S2), 6 mM (S3), 9 mM (S4) or 12 mM (S5).

An aliquot of 20 μL of test solution was applied to the surface of ImA or ImG. The yellow color development was monitored up to 5 minutes from the start of reaction. Color changes were captured every 30 second by smartphone camera, with an LED light as the only light source and at a constant distance between the sample and the camera.

2.5. The effect of washing

The one paper cyrcle was immersed in 3 mL of PB for 2 minutes at 25 ºC. After that, it was withdrawn and

transferred to a clean cuvette for the residual activity measurement, or it was subjected to a next washing cycle with new portion of 3 mL PB. The washing PB solutions from all washing cycles performed on one immobilizate (up to 4 cycles) were also collected for subsequent activity determination. The percentage of the residual activity was calculated considering the activity of the unwashed sample as 100%.

2.6. The effect of sample matrix on visual response

An aliquot of 20 μL of PB was applied to the surface of ImA or ImG and allowed to spread and absorb for defined time. Subsequently, the visual response of the immobilizate was monitored using a test solution with DTNB (4 mM) and BSChI (6 mM), as described in the Section 2.4.

3. RESULTS AND DISCUSSION

3.1. Temperature effects on activity and stability

In the immobilization process, the aliquots of enzyme solution with 1 % BSA (217 ± 6 mU) or 0.5 % gelatin (213 ± 7 mU) were used to obtain immobilizates ImA and ImG. Under the conditions defined by the assay method, ImA and ImG showed activities of 95 ± 5 mU and 53 ± 4 mU, so activity yields of 44% and 25% were achieved, respectively.

Temperature-induced changes in the properties of the obtained immobilizates were studied in two different scenarios. In the first, bioactive paper was in a dry state, surrounded by ambient air in a closed vessel that was placed in an oven. In the second, it was immersed in a cuvette filled with PB and placed in a water bath.

In an attempt to assess the influence of a similar temperature oscillation during storage conditions, after heat treatment at 55 ºC for 2 hours the vessels and cuvettes with the tested samples were left for an additional 2 hours at room temperature to slowly cool down.

The activity measurements were performed on a dry sample taken from a vessel treated in an oven, on a sample removed from a cuvette treated in a water bath and on PB remaining after sample removal. Also, additional samples were subjected to treatment in a water bath to measure the activity of the total contents of the cuvette (sample immersed in PB) (**Table 1**).

The results showed that none of the stabilizers protected the immobilizates from activity decline under the tested conditions. However, the thermal effects on dry samples were more severe on ImG, and the presence of BSA in ImA samples appears to be more beneficial for retaining the BChE activity at high temperatures.

Table 1. The residual activities of the samples and PB after heat treatment (starting activities of ImA and ImG are shown at the first row)

Sample	ImA		ImG	
	mU	%	mU	%
before heat treatment	95 ± 5	100	53 ± 4	100
from a vessel after oven	59 ± 3	62	11 ± 3	20
from a cuvette after water bath	< 1	< 1	< 1	1
PB only after water bath	79 ± 2	83	66 ± 1	123
paper and PB after water bath	75 ± 2	79	64 ± 2	120

The activities of all samples treated in the water bath and withdrawn from PB were negligible, and the results on the activities remaining in PB after samples removal confirmed the enzyme leakage from the support to an almost the same extent with both ImA and ImG. That is visually more noticeable at **Figure 1**, where all activities are presented in normalized form, with a value of 100% assigned to the initial activity of free enzyme in the starting enzyme solution used for immobilization.

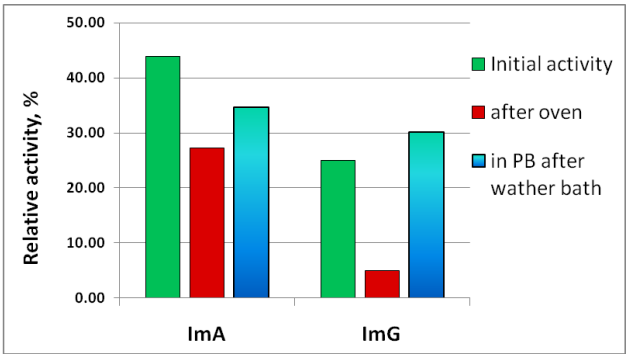

Figure 1. The influence of tempereture on ImA, ImG and their incubation PB after different incubating conditions, relative to the initial activity of the free enzyme

An additional experiment was performed to test the stability of samples immersed in PB without heat treatment. Cuvettes with ImA and ImG immersed in PB were left at room temperature for 4 hours. The activities remaining in PB after removal of ImA and ImG were 163 ± 8 mU and 113 ± 2 mU, while activities remaining at papers were less than 2 mU and 4 mU, respectively. The obtained results imply that the presence of gelatin contributes more to the enzyme stability from the aspect of leakage, but also that the enzyme leakage, regardless of the temperature conditions, is a characteristic property of the immobilizates resulted from the applied immobilization procedure.

3.2. The visual response's dependency on substrate concentration

The activity of paper-immobilized BChE can be visually evaluated in different reaction systems, and one of the most used is based on the yellow color produced by the enzymatic reaction according to Ellman's method. The analytical performances of the obtained bioactive papers were examined at five different substrate concentrations with test solutions S1- S5. The visual responses of ImA and ImG upon addition of test solutions were digitally recorded, and their images up to 5 minutes from the start of the reaction are shown in **Figure 2**. The resulting color on the samples surfaces changed from colorless to yellow at a rate that was higher with increasing BSChI concentration and the most noticeable differences in color intensity were achieved during the first two minutes. Increasing the concentration of BSChI above 6 mM (S3) had a minor visual effect that was only visible with ImA.

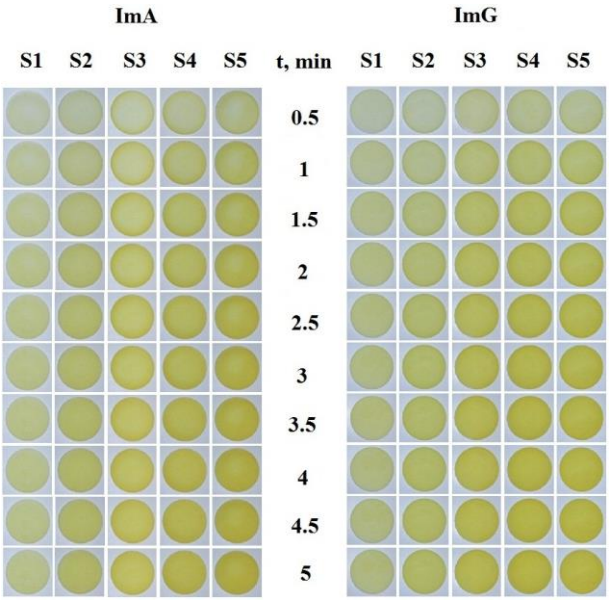

Figure 2. Comparative display of color development on ImA and ImG depending on reaction time at different substrate concentrations in test solutions S1 – S5

Considering the dependence of the yellow color intensity on the enzyme loading on paper and the fact that the visual responses of ImA and ImG were practically the same, it is conclusive that lower activity yield of ImG is a consequence of some limitations that are relevant under the assay conditions, but not when the substrate is applied directly to ImG surface. Among other reasons, this could originate from the differences between liquid transport mechanism in a porous substrate immersed in a liquid medium and the process of droplet absorption from the porous substrate surface.

3.3. The effect of washing

The samples of ImA and ImG were washed by repeated immersion in 3 mL of PB for 2 minutes and the residual activities on the paper circles were monitored for up to four washing cycles. **Table 2** summarizes the measured activities of ImA and ImG.

Table 2. The residual activities of ImA and ImG after washing cycles

No. of washing cycles	ImA		ImG	
	mU	%	mU	%
-	95 ± 5	100	53 ± 4	100
1	28 ± 1	29	19 ± 2	36
2	17 ± 2	18	20 ± 1	37
3	12 ± 1	13	11 ± 2	20
4	9 ± 1	9	10 ± 2	19

The results confirmed that most of the enzyme molecules on the surfaces of ImA and ImG samples were only loosely bound or unbound and therefore released rapidly upon immersion in the PB. Most of the enzyme activity was lost during the first washing cycle, after which both samples retained approximately 30 % of their initial activity. With subsequent washing steps, the activity of ImA gradually decreased, remaining at less than 10 % after the forth washing cycle, while the activity of ImG decreased in a stepwise manner to approximately 20 %. After the second washing cycle, both ImA and ImG had a similar number of enzyme units measured in conditions defined by the assay method, and the same trend was maintained until the forth washing cycle. The effects of enzyme loss by washing ImA and ImG samples shown in **Figure 3** reveal the dominance of weakly bound enzyme on the immobilizate prepared in the presence of BSA.

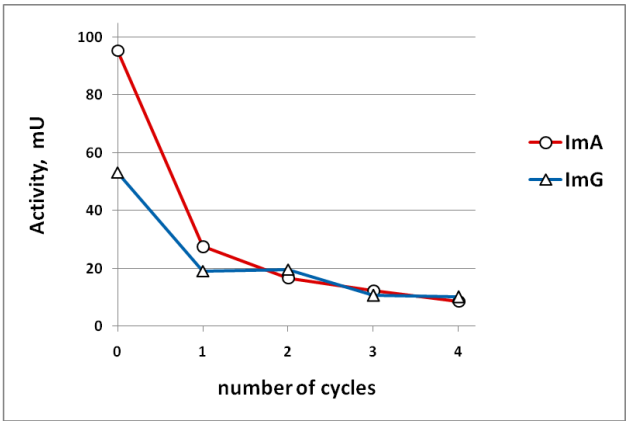

Figure 3. The activity of ImA and ImG samples depending on the number of washing cycles performed

The activities of the buffer solutions collected during washing steps are shown in **Table 3**. The total amount of enzyme units released from ImA after four consecutive washing cycles was twice the number of enzyme units released from ImG, providing further support for the observation that BChE is better retained when immobilized in the presence of gelatin.

To study the effects of washing on ImA and ImG performances related to their visual responses, the immobilizates obtained after one washing cycle were subjected to color reaction by addition of test solution with 6 mM BSChI (S3) and color development was monitored as described in the Section 2.4. **Figure 4**

compares the visual effects of unwashed ImA and ImG samples versus the samples obtained after one cycle of washing.

Table 3. The total activities of washing PB after washing cycles performed on ImA and ImG samples

No. of washing cycles	washing PB of ImA		washing PB of ImG	
	mU	%	mU	%
1	64 ± 5	67	11 ± 6	21
2	105 ± 13	110	34 ± 2	64
3	99 ± 8	104	41 ± 8	76
4	116 ± 7	122	55 ± 7	103

Upon one cycle of washing, the color on ImA sample developed slowly and had a low intensity and uneven distribution until the end of the fifth minute from the start of the reaction, which led to the conclusion that this immobilizate is not suitable for the application by immersion into the testing liquid.

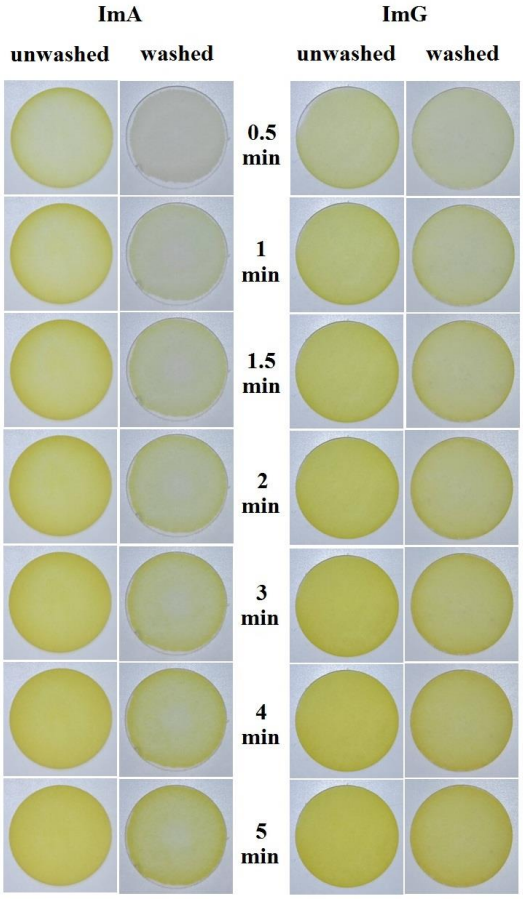

Figure 4. Comparison of color development on unwashed and washed ImA and ImG samples

Unlike washed ImA sample, ImG after washing still provided observable color changes that occurred at a slower rate than in unwashed sample, but with uniform color distribution and intensity that developed to an appropriate level during reaction monitoring.

3.4. The effect of sample matrix on visual response

The simple devices for visual detection of ChEs inhibitors are mostly intended to be used by applying a certain volume of the testing liquid sample directly to the surface of the detector's sensing zone and allowing the eventual inhibition reaction to occur for some time. For a reliable analysis of the results, it is important to know all the possible influences that the sample matrix can have on the obtained visual responses. Among the various physico-chemical changes that can arise from samples of different composition, the effects of the PB on visual responses of ImA and ImG, if any, should be the least pronounced. But when applied on the surfaces of ImA and ImG, PB affected the visual responses of immobilizates and its influence was dependent on the time elapsed until the addition of the test solution with DTNB and BSChI. The effects of the incubation with PB for 2 minutes and 15 minutes before the onset of the visual reaction are shown in **Figure 5.**

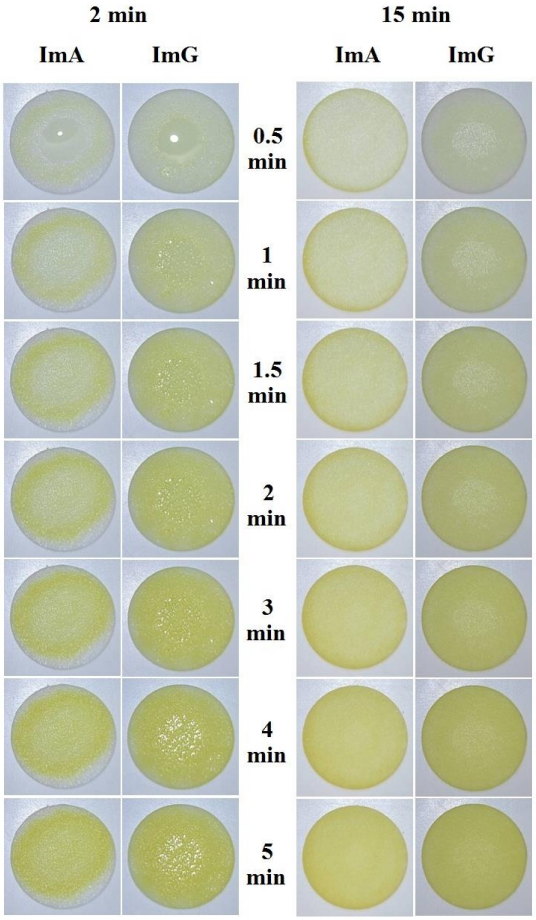

Figure 5. Visual responses of ImA and ImG when the test solution S3 was applied after 2 minutes or 15 minutes incubation with PB

Images taken when the reaction started after 2 minutes of incubation with PB showed slow absorption of the liquid droplet, partial coloring of ImA and reflection from the wetted surface of ImG, all of which made them unsuitable for further data processing using appropriate image analysis software, therefore unusable for the objective

evaluation of the obtained results. These effects disappeared with increasing incubation time, as can be seen in the images taken when the visual responses were initiated after 15 minutes of incubation with PB.

4. CONCLUSION

The immobilization of BChE was carried out by simple deposition method using enzyme solutions with BSA or gelatin as stabilizers and Whatman No. 1 paper as support. The properties of the resulting immobilizates (ImA or ImG, respectively) were examined from a few aspects relevant for biodetection applications.

The immobilized BChE was characterized by a fast and visible color change that was most noticeable during the first two minutes after contact with the solution containing the indicator (4 mM) and the substrate in concentrations of 6 mM or higher, and also by practically the same yellow color intensity on the surfaces of ImA and ImG. Both immobilizates were prone to enzyme desorption and leakage owing to abundance of loosely bound and unbound enzyme molecules, which was expected for the applied immobilization procedure. According to visual responses of samples subjected to one washing cycle of 2 minutes in PB, ImA was found to be unsuitable for visual detection purposes by immersion in the sample due to inhomogeneous and weak color intensity, while after the same treatment ImG still provided adequate visual readouts with uniform color distribution. Tests with the application of PB as a sample matrix expected to have the least adverse effect, confirmed that the use of ImA and ImG in detection by the sample deposition method is highly dependent on the incubation time, which is essential for the uniform liquid distribution and thus for obtaining useful visual responses that can be further processed. The temperature-induced activity decrease was less pronounced in ImA when the samples were stored in dry form.

The application of physical immobilization techniques in the fabrication of simple analytical devices for visual screening and monitoring of ChEs target analytes is favorable due to their low-cost and simplicity, but the drawbacks, which are mainly caused by week bonds between the enzyme and the support, usually affect the performances of the resulting analytical tools. The characterization of the immobilized ChE as their biorecognition element is a necessary step for establishing the direction of further improvements, since the immobilized enzymes properties are crucial for defining the possibilities and limitations of their use.

References

[1] ŠTĚPÁNKOVÁ, Š., VORČÁKOVÁ, K.: *Cholinesterase-based biosensors*, Journal of Enzyme Inhibition and Medicinal Chemistry, 31 (2016) 180–193.

[2] SOLDATKIN, O. O. et al.: *Application of butyrylcholinesterase-based biosensor for simultaneous determination of different toxicants using inhibition and reactivation steps*, Electroanalysis, 36 (6) (2024) e202300400.

[3] AYAZ, S. et al.: *A novel acetylcholinesterase inhibition based colorimetric biosensor for the detection of paraoxon ethyl using CUPRAC reagent as chromogenic oxidant*, Talanta, 266 (2024) 124962.

[4] TSOUNIDI, D. et al.: *AChE-based electrochemical biosensor for pesticide detection in vegetable oils: matrix effects and synergistic inhibition of the immobilized enzyme*, Analytical and Bioanalytical Chemistry, 415 (4) (2023) 615-625.

[5] ISSAKA, E. et al.: *Advanced visual sensing techniques for on-site detection of pesticide residue in water environments*, Heliyon, 9 (3) (2023) e13986.

[6] BŘÍZOVA, A., PITSCHMANN, V.: *Simple Chemical and Cholinesterase Methods for the Detection of Nerve Agents Using Optical Evaluation*, Biosensors, 13 (12) (2023) 995.

[7] XUE, J. et al.: *Portable sensors equipped with smartphones for organophosphorus pesticides detection*, Food Chemistry, 434 (2024) 137456.

[8] VINOTHA ALEX, A., MUKHERJEE, A.: *Review of recent developments (2018-2020) on acetylcholinesterase inhibition based biosensors for organophosphorus pesticides detection*, Microchemical Journal, 161 (2021) 105779.

[9] WU, Y. et al.: *Sensitive inkjet printing paper-based colorimetric strips for acetylcholinesterase inhibitors with indoxyl acetate substrate*, Talanta, 162 (2017) 174-179.

[10] TSAGKARIS, A.S. et al.: *A microfluidic paper-based analytical device (μPAD) with smartphone readout for chlorpyrifos-oxon screening in human serum*, Talanta, 222 (2021) 121535.

[11] ELLMAN, G. L., COURTNEY, K. D., ANDERS, V., FEATHERSTONE, R. M.: *A new and rapid colorimetric determinaton of acetylcholinesterase activity*, Biochemical Pharmacology, 7 (2) (1961) 88–95.

11TH INTERNATIONAL SCIENTIFIC CONFERENCE
ON DEFENSIVE TECHNOLOGIES
OTEH 2024
Serbia, Tara, 9-11 October 2024

MAGNETOIMPEDANCE EFFECT OF NANOCRYSTALLINE FeNiSiB and FeCuVSiB RIBBONS

RADOSLAV SURLA
Military Technical Institute, Belgrade, Serbia, ekorade@gmail.com

MILICA M. VASIĆ
Faculty of Physical Chemistry, University of Belgrade, Belgrade, Serbia, mvasic@ffh.bg.ac.rs

DRAGICA M. MINIĆ
Faculty of Physical Chemistry, University of Belgrade, Belgrade, Serbia, dminic@ffh.bg.ac.rs

LJUBICA RADOVIĆ
Military Technical Institute, Belgrade, Serbia, ljubica.radovic@mod.gov.rs

NEBOJŠA MITROVIĆ,
Faculty of Technical Sciences, University of Kragujevac, Serbia, nebojsa.mitrovic@ftn.kg.ac.rs

PAVEL CRNOMARKOVIĆ,
Military Technical Institute, Belgrade, Serbia, pavel@ptt.rs

Abstract: *The Magnetoimpedance (MI) effect of Fe-based nanostructured alloy ribbons $Fe_{72}Ni_8Si_{10}B_{10}$ (A) and $Fe_{72}Cu_1V_4Si_{15}B_8$ (B) was studied, compared for the two ribbons, and finally correlated with their composition and microstructure. The nanostructured ribbons were prepared by melt-spinning on a cold rotating disk. Basic characterization of the studied ribbons was performed by XRD and SEM-EDX techniques. It was found that the MI ratio of ribbon A is significantly lower than that of ribbon B, but the effects were observed at different frequencies. The maximal MI ratio of ribbon A was detected at 57.57 MHz, while in the case of ribbon B, that was the frequency of about 13 MHz. The structure of both ribbons consists of a certain amount of nanocrystals, α-(Fe, Ni) for the ribbon A and α-Fe(Si) for the ribbon B, which are embedded in an amorphous matrix. The MI effect and the frequency of its maximum are determined by the mobility of the magnetic domains in the samples, which is correlated with the microstructural specificities of individual ribbons.*

Keywords: *Magnetoimpedance effect, nanostructure, melt-spinning, α-Fe(Si), α-(Fe, Ni)*

1. INTRODUCTION

Magnetoimpedance (MI) effect is defined as the influence of external DC field on the change in impedance of ferromagnetic sample. It was discovered at the beginning of the last decade of the twentieth century, and nowadays, it is applied in magnetic field sensors with high sensitivity [1-5]. Some ferromagnetic amorphous / nanocrystalline alloys were found to exhibit the MI effect.

The impedance of ferromagnetic material declines with an increase in magnetic field, but on the other hand, it grows with an increase in the frequency of the current flowing through the sample.

Most commonly, the MI ratio is expressed using the following equation:

$$\Delta Z/Z(\%)=100\% \cdot(Z(H)-Z(H_{max}))/Z(H_{max}), \quad (1)$$

where $Z(H_{max})$ is impedance at the maximum value of external magnetic field. Depending on the material considered, at H=0, the remanent magnetization can affect the impedance, and further, with increase in magnetic field, such magnetization become annulled, resulting in asymmetry of MI-diagram for different magnetic field directions (–H and +H).

The dependence of magnetoimpedance on frequency is related to the skin effect. This effect is characterized by penetration depth, which grows with an increase in magnetic field (due to decrease in magnetic permeability), and decline with increase in frequency. Alternating current causes the occurrence of eddy currents, which include the grouping of charges that transmit the electrical energy to the peripheral parts of the conductor. The skin depth can be defined as:

$$\delta_m=(\rho/(\pi\cdot\mu\cdot f))^{-1}, \quad (2)$$

where ρ is specific electrical resistivity, μ is magnetic permeability, and f is frequency.

Beside the aforementioned, the MI ratio depends on the

Corresponding author: R. Surla;
E-mail: ekorade@gmail.com
DOI: 10.5937/OTEH24098S

domain structure of magnetic material, which is determined by the material composition and microstructure, and is closely related to the preparation technology.

The maximal MI ratio occurs at specific values of external magnetic field and frequency of the current flowing through the sample. It can be determined experimentally, and it is tightly related to the microstructure of the material.

2. EXPERIMENTAL PROCEDURE

In this work, the $Fe_{72}Ni_8Si_{10}B_{10}$ ribbon-shaped alloy (A) was subjected to experimental measurements of magnetoimpedance, and then compared with our previous MI research [4, 6] of the $Fe_{72}Cu_1V_4Si_{15}B_8$ ribbon (B). The ribbon-shaped alloys, 1.5 mm wide, were prepared by melt-quenching, which included rapid cooling of the melt on a cold wheel rotating at 2000 rpm. The average thickness of the alloys A and B is around 55 μm [7].

Microstructure of the studied alloys was examined by means of X-ray diffraction analysis (XRD). For this purpose, a Rigaku SmartLab diffractometer equipped with a Cu Kα radiation source was used. Rietveld refinement was conducted to estimate the contents and microstructural parameters of individual phases in the samples. Scanning electron microscopy (SEM), with a SEM JEOL JSM-6610-LV microscope, was carried out to examine the surface morphology of the samples (shiny side).

In order to study the magnetoimpedance effect of the ribbons, measurements of the impedance were performed in homogeneous magnetic field of 15 kA/m, generated using the pair of Helmholtz coils, with an instrument Vector Network Analyser Agilent 8753ES. The sample holder was specially designed to allow measurements on the ribbon-shaped samples, 1 cm in length.

3. RESULTS AND DISCUSSION

3.1 XRD analysis

XRD analysis of the as-cast alloy ribbons reveals the composite structure, including the presence of crystalline phases in the samples, beside the amorphous matrix, Figures 1 and 2.

The abundance of crystalline grains inside the ribbon is not homogeneous due to differences in cooling rates occurring during the ribbon preparation. Namely, the wheel-side of the ribbon (matte side) is cooled faster and thus solidificates faster than the opposite (shiny) side, resulting in larger crystalline fraction at the shiny side of the ribbon, Table 1.

Figures 1 and 2 represents the XRD patterns of the A and B alloy ribbons, respectively, indicating the alloy structure consisted of bcc iron (α) crystals embedded in amorphous matrix. The bcc iron phase is denoted as α-(Fe, Ni) and α-Fe(Si) in the case of A and B, respectively, Figures 1 and 2, considering the solubility of Si and Ni elements in the bcc iron structure.

The average crystallite size of the bcc iron phase was estimated from the XRD patterns for both ribbons, amounting to 53 and 40 nm for A and B, respectively.

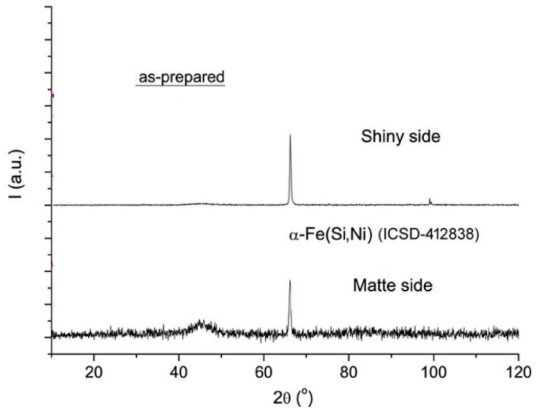

Figure 1. XRD patterns of the $Fe_{72}Ni_8Si_{10}B_{10}$ (A) alloy ribbon.

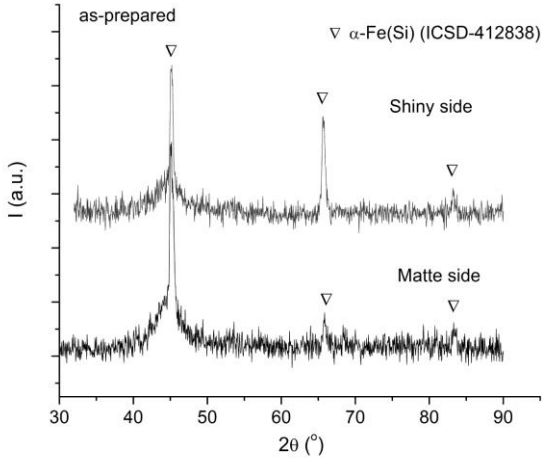

Figure 2. XRD patterns of the $Fe_{72}Cu_1V_4Si_{15}B_8$ (B) alloy ribbon.

Table 1. Weight fraction of the bcc iron crystalline structure at matte and shiny sides of the studied ribbons.

Ribbon	Matte side	Shiny side
$Fe_{72}Ni_8Si_{10}B_{10}$ (A)	5 wt.%	14 wt.%
$Fe_{72}Cu_1V_4Si_{15}B_8$ (B)	18 wt.%	20 wt.%

3.2 SEM analysis

Relatively uniform surface morphology of both ribbons, A and B, can be observed in the SEM micrographs presented in Figures 3 and 4. Some dents at the surface of the ribbons resulted from the preparation procedure, including melt quenching.

EDX analysis, performed in the regions marked on the micrographs, confirmed the presence of the elements

specified in the alloy designation, at the ribbon surface, Table 2.

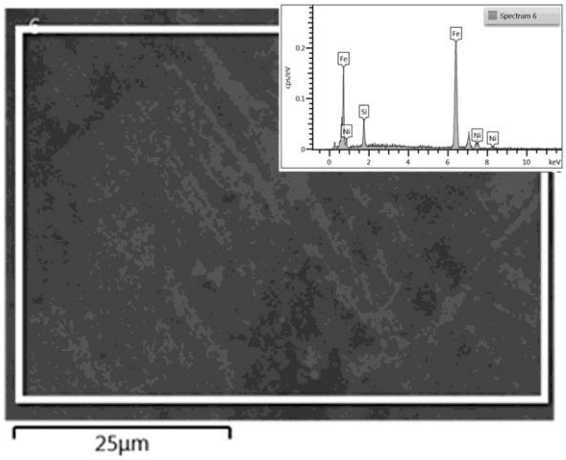

Figure 3. SEM micrograph (with EDX spectrum) of the as-cast $Fe_{72}Ni_8Si_{10}B_{10}$ (A) alloy ribbon.

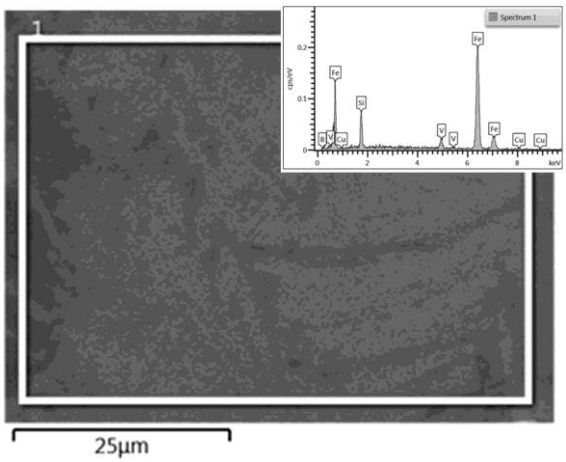

Figure 4. SEM micrograph (with EDX spectrum) of the as-cast $Fe_{72}Cu_1V_4Si_{15}B_8$ (B) alloy ribbon.

Table 2. Results of the EDX analyses (at. %) performed for the alloy ribbons studied in the work.

	Fe	Ni	Si	
$Fe_{72}Ni_8Si_{10}B_{10}$	79.3	9.6	11.1	
	Fe	Cu	V	Si
$Fe_{72}Cu_1V_4Si_{15}B_8$	79.1	1.1	4.5	15.3

3.3. Magnetoimpedance measurements

The MI ratio of the $Fe_{72}Ni_8Si_{10}B_{10}$ (A) alloy ribbon at various frequencies and magnetic fields was studied, and the obtained results are presented in Figures 5-8. The maximal MI ratio, 26%, is observed for frequencies 57-58 MHz (MI_{max}= 26% for f= 57.57 MHz and H= 847.2 A/m, while H_{max}=15kA/m).The dependence of MI ratio of A on frequency for various magnetic field values is presented in Figures 5 and 6. The effect grows with increase in magnetic field up to 847.2A/m (Figure 5), while further increase in magnetic field leads to decline in the MI ratio (Figure 6).

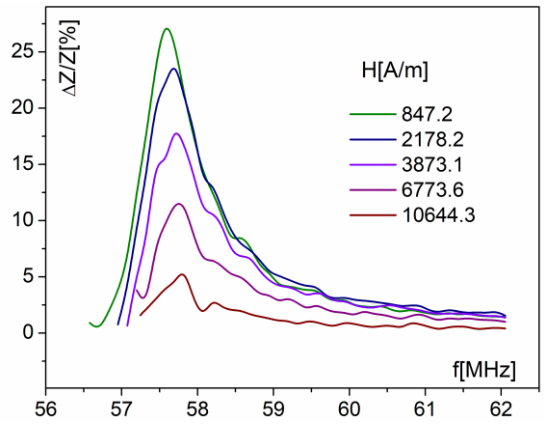

Figure 5. Dependence of MI ratio of $Fe_{72}Ni_8Si_{10}B_{10}$ (A) alloy ribbon on frequency for magnetic field ranging 0-847.2 A/m; H_{max}=15 kA/m.

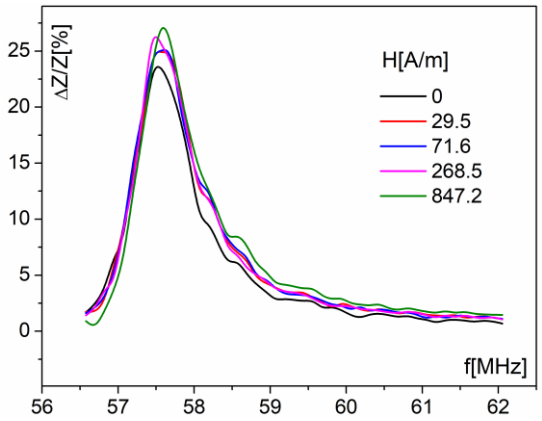

Figure 6. Dependence of MI ratio of $Fe_{72}Ni_8Si_{10}B_{10}$ (A) alloy ribbon on frequency for magnetic field ranging 847.2-10644 A/m; H_{max}=15 kA/m.

Figures 7 and 8 show the dependence of MI ratio of A on magnetic field for characteristic frequencies. The growth of the MI ratio with frequency up to f= 57.57 MHz, Figure 7, and decline of the MI ratio with further increase in frequency (f > 57.57 Hz, Figure 8) can be observed.

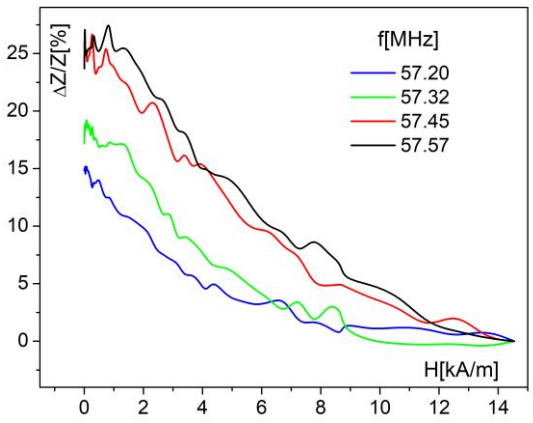

Figure 7. Dependence of MI ratio of $Fe_{72}Ni_8Si_{10}B_{10}$ (A) alloy ribbon on magnetic field for frequency ranging 57.2-57.57 MHz; H_{max}=15 kA/m.

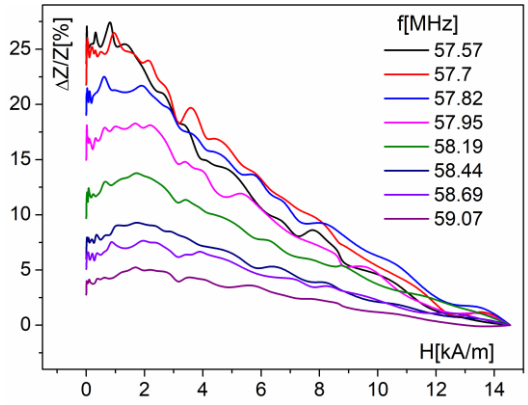

Figure 8. Dependence of MI ratio of $Fe_{72}Ni_8Si_{10}B_{10}$ (A) alloy ribbon on magnetic field for frequency ranging 57.57-59.07 MHz; H_{max}=15 kA/m.

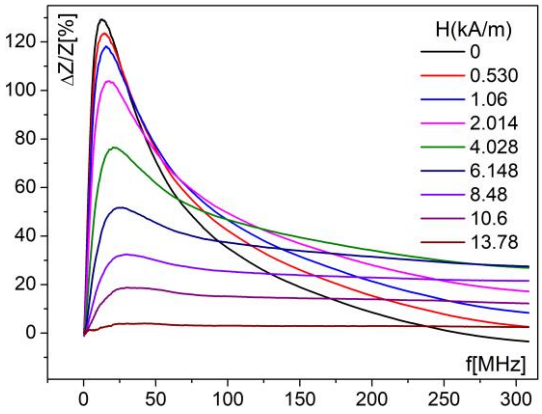

Figure 9. Dependence of MI ratio of $Fe_{72}Cu_1V_4Si_{15}B_8$ (B) alloy ribbon on frequency for positive magnetic field ranging 0-13.8 kA/m; H_{max}=14.8 kA/m.

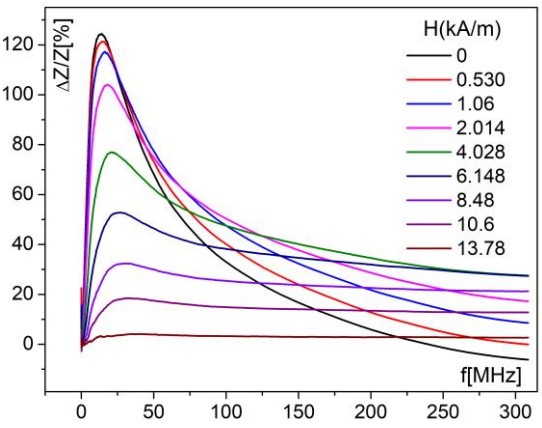

Figure 10. Dependence of MI ratio of $Fe_{72}Cu_1V_4Si_{15}B_8$ (B) alloy ribbon on frequency for negative magnetic field ranging 0-13.8 kA/m; H_{max}=14.8 kA/m.

The maximal MI ratio of the $Fe_{72}Cu_1V_4Si_{15}B_8$ (B) alloy ribbon, obtained for H_{max} of around 15 kA/m, amounts to 125-129% (129% for f= 13 MHz, H= 0 and + direction, and 125% for f= 12.5 MHz, H= 106 A/m and - direction), Figures 9-12, and it is several times larger than that of the ribbon A. By the way, our previous research of the ribbon B [4] revealed MI_{max}= 153%, but for H_{max}=21.2 kA/m (f= 18.55 MHz and H= 0 A/m).

Better MI ratio of the ribbon B than that of the ribbon A can be attributed to better mobility of magnetic domains in the case of B, which is related to the microstructure and composition of the material. Crystal size is very important microstructural parameter, where it is thought that the nanocrystal size lower than the magnetic exchange length considerably reduces the contribution of magnetocrystalline anisotropy of the nanocrystals to the overall magnetic anisotropy of the material [8, 9], affecting its overall magnetic behavior. For Fe-based alloys, the ferromagnetic exchange length is 20-40 nm [10]. For the studied alloy ribbons, A and B, certain difference in the crystallite size of the bcc iron phase is observed (53 nm for A, and 40 nm for B), which has an effect on the average anisotropy, considering its proportionality to the sixth power of the crystal size [10]. For the crystals formed in the as-cast ribbons, the crystallite size is connected with the chemical composition of the alloy. In the B ribbon, Cu and V elements are present, where Cu makes the nucleation process faster and V decreases the crystal growth rate, thus yielding lower crystallite size than that of the Fe-based alloys without such additives, while similar components are not present in the ribbon A.

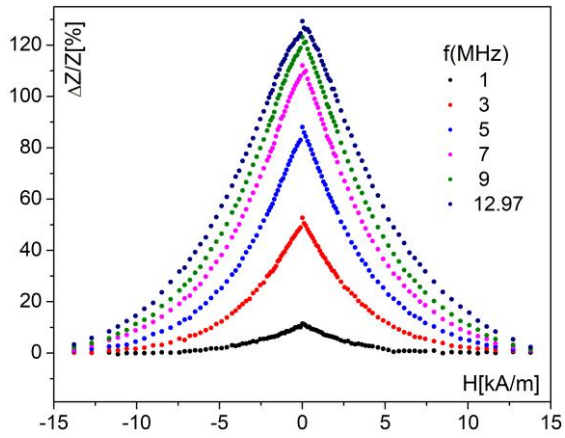

Figure 11. Dependence of MI ratio of $Fe_{72}Cu_1V_4Si_{15}B_8$ (B) alloy ribbon on magnetic field for frequency ranging 1-13 MHz; H_{max}= ±14.8 kA/m.

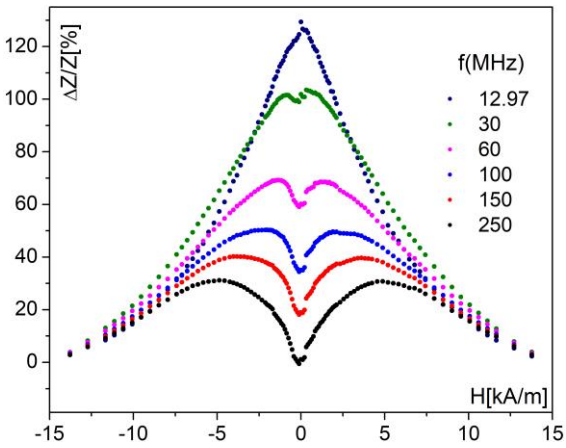

Figure 12. Dependence of MI ratio of $Fe_{72}Cu_1V_4Si_{15}B_8$ (B) alloy ribbon on magnetic field for frequency ranging 13-250 MHz; Hmax= ±14.8 kA/m.

5. CONCLUSION

The magnetoimpedance effect is observed for both alloys studied in this work, suggesting their potential application in MI sensors. The effect is more pronounced for the $Fe_{72}Cu_1V_4Si_{15}B_8$ (B) alloy, and thus its magnetoimpedance sensitivity to an external magnetic field is larger. The MI effect of the $Fe_{72}Ni_8Si_{10}B_{10}$ (A) is weaker and occurs at higher frequencies. The MI effect is significantly dependent on the microstructure of the materials. The microstructure consisted of the bcc iron (α) crystals embedded in amorphous matrix is crucial for the magnetic behavior of both alloys. Appropriate choice of chemical composition of the material and preparation conditions allow the production of alloy ribbons with desired microstructure, and thus the design of materials with targeted properties, in this case potentially applicable in the MI elements.

Acknowledgments

This work was supported in part by the Ministry of Science, Technological Development and Innovation of the Republic of Serbia, Faculty of Technical Sciences Čačak, University of Kragujevac under Grant 451-03-66/2024-03/200132, Faculty of Physical Chemistry, University of Belgrade, under Grant 451-03-66/2024-03/200146, and Military Technical Insitute under grant 451-03-66/2024-03/200325.

References

[1] Panina, L.V., Mohri, K.: *Magneto-impedance Effect in Amorphous Wires*, Applied Physics Letters, 65(9), (1994), 1189 – 1191.

[2] Kraus, L.: *Theory of Giant Magneto-impedance in the Planar Conductor with Uniaxial Magnetic Anisotropy*, Journal of Magnetism and Magnetic Materials, 195(3), (1999), 764 – 778.

[3] Surla, R., Mitrović, N., Đukić, S., Ibrahimović, V.: *Amorphous $Fe_{72}Cu_1V_4Si_{15}B_8$ Ribbon as Magneto-Impedance Sensing Element*, Serbian Journal of Electrical Engineering, 13(3), (2016), 381-394.

[4] Surla, R., M., Vasić, Mitrović, N., Radović, Lj., Minić, D.: *Magnetic properties of* $Fe_{72}Cu_1V_4Si_{15}B_8$ *alloy with a composite amorphous/ nanocrystalline structure*, Journal of Magnetism and Magnetic Materials, 564 (2022) 170141

[5] SURLA, R.: Doktorska disertacija: *Uticaj odgrevanja na strukturne transformacije i magnetna svojstva legure $Fe_{72}Cu_1V_4Si_{15}B_8$*, FTN Čačak, Univerzitet u Kragujevcu, 2021.

[6] Vasić M., Surla R., Mitrović N., Minić Dragica., Mitrović N., Maričić A., Minić Dušan: *Thermally induced microstructural transformations of $Fe_{72}Cu_1V_4Si_{15}B_8$ alloy*, Metal. Mater. Trans. A 48 (2017) 4393–4402.

[7] Surla, R., M., Vasić, Mitrović, N., Minić, D.: *Synthesis and characterization of $Fe_{72}Cu_1V_4Si_{15}B_8$ metallic glass ribbons prepared by melt spinning casting*, 9th International Scientific Conferenceon Defensive Technologies, Belgrade, 8-9, October 2020.

[8] Herzer, G.: *Grain structure and magnetism of nanocrystalline ferromagnets*, IEEE Transactions on Magnetics, 25 (1989) 3327-3329.

[9] Kulik, T.: *Nanocrystallization of metallic glasses*, Journal of Non-crystalline Solids, 287 (2001) 145-161.

[10] Herzer, G.: *Anisotropies in soft magnetic nanocrystalline alloys*, Journal of Magnetism and Magnetic Materials, 294 (2005) 99-106.